

Planetary nebulae as kinematic tracers of galaxy stellar halos

Lodovico Coccato

European Southern Observatory, Karl-Schwarzschild Strasse 2, D-85748 Garching, Germany.
email: lcoccato@eso.org

Abstract. The kinematic and dynamical properties of galaxy stellar halos are difficult to measure because of the faint surface brightness that characterizes these regions. Spiral galaxies can be probed using the radio HI emission; on the contrary, early-type galaxies contain less gas, therefore alternative kinematic tracers need to be used. Planetary nebulae (PNe) can be easily detected far out in the halo thanks to their bright emission lines. It is therefore possible to map the halo kinematics also in early-type galaxies, typically out to 5 effective radii or beyond. Thanks to the recent spectroscopic surveys targeting extra-galactic PNe, we can now rely on a few tens of galaxies where the kinematics of the stellar halos are measured. Here, I will review the main results obtained in this field in the last decades.

Keywords. galaxies: general; galaxies: haloes; galaxies: kinematics and dynamics; ISM Planetary Nebulae: general.

1. Introduction

The study of kinematics and chemical content in the outer regions of galaxies is extremely important to understand dynamics, dark matter content and distribution, and to get constrain on formation processes of the galaxies themselves. Indeed, the dynamical timescale of the stellar halos is comparable to the age of the galaxy (e.g., Binney & Tremaine 1987), therefore the imprints of formation processes can be still be preserved in the mass and orbital distribution and stellar population properties.

The challenge of these studies resides in the faint surface brightness level of the stellar halos. Indeed, either traditional long-slit or integral field absorption line spectroscopy require long integration times to go beyond 2 effective radii (e.g., Coccato et al. 2010a,b, 2011; Greene et al. 2012, 2015). This is particularly challenging for early-type galaxies because, contrarily to their spiral counterparts, they do not contain as much gas to be used as kinematic tracer in their outskirts.

Using planetary nebulae (PNe) as alternative tracer for the kinematics of the underlying stellar population revealed to be a winning strategy. Indeed, PNe can be detected far out in galaxy halos, thanks to their bright [O III] $\lambda 5007$ emission line that outshines the stellar continuum background. The idea has been exploited by many groups, targeting a large variety of nearby galaxies including our own. The basic strategy includes the identification of the PNe candidate (e.g., by means of multi band photometry) and their spectroscopic follow-up to get the radial velocity and, eventually, emission line ratios for chemical studies. Because this two-stages approach can include a number of systematic effects (e.g. change of observing conditions between exposures), a dedicated instrument was build: Planetary Nebulae Spectrograph (PN.S, Douglas et al. 2002). The PN.S exploits the simultaneous counter-dispersed imaging technique, which allows to identify and obtain the radial velocity of a PNe in a single exposure.

The purpose of this review is to highlight the main results in obtained by using PNe as kinematic tracers in the last decades.

2. Measuring the distribution and kinematics of the PNe population

The first thing that needs to be done to establish if PNe are indeed useful to extend the information of stars to larger radii is to check whether or not the PNe represent the properties of the underlying stellar population in the regions where their observations overlap. This is done in two ways: by comparing the number density of PNe with the stellar surface brightness profiles (Section 2.1), and by comparing the stellar kinematics with the one derived from absorption line spectroscopy (Section 2.2).

2.1. *Spatial distribution of PNe*

The most common way to compare the PNe density distribution and stellar surface brightness is divide the galaxy into concentric annuli, count the PNe within each annuls, and compare the number density (counts divided by area) to the mean stellar surface brightness in that area. One important aspect to consider is the completeness of the sample, which can be established by populating the original image with simulated sources and re-run the PNe detection procedure. The number density of PNe needs to be corrected for incompleteness before being compared to the stellar surface brightness. The scaling factor between light and PNe counts is related to the PNe specific frequency (the so-called α parameter, Jacoby 1980); see for example Arnaboldi (2012) for a review.

2.2. *Kinematics*

Unlike absorption line spectroscopy, in which the kinematics measured at a given position *is* the luminosity weighted kinematics of all the stars along that line of sight, the velocity of a given PN represents that object only, and does not necessarily reflect the mean behaviour of the population. In other words, a single PNe velocity determination is like a “random number” extracted from the line-of-sight velocity distribution. Thus, it is necessary to proceed on a statistical way, and use the combined information of many PNe around a given area to “reconstruct” the mean kinematics (velocity and velocity dispersion) of that area. Then, one can compare the kinematics obtained from stars and PNe in the regions where both tracers are available.

Several techniques have been developed either to reconstruct the 2D velocity kinematics or to use the individual velocities in dynamical models (Romanowsky & Kochanek 2001; Amorisco & Evans 2012; Foster et al. 2013; Arnold et al. 2014). Here we focus on the “Gaussian Kernel smoothing” technique developed in Peng et al. (2004), with “Adaptive Kernel” as introduced in Coccato et al. (2009). Basically, the kinematics at each point in the field of view is obtained computing weighted moments of the velocity distribution of the entire PNe population. Each PN contributes with a weight that depends on its distance to that point. The weights dependency from distance is a Gaussian function, where its dispersion (kernel amplitude) depends on the local density of PNe. Regions with high PNe density have smaller kernel amplitude, regions with low PNe density have larger kernel amplitude. Figure 1 compares the two-dimensional map of individual PN velocities with the two-dimensional maps of velocity and velocity dispersions reconstructed using this technique.

2.3. *Comparison between stellar and PNe properties*

The comparison between stars and PNe revealed that the distribution and kinematics of PNe is in good agreement with the stellar surface brightness and kinematics in the

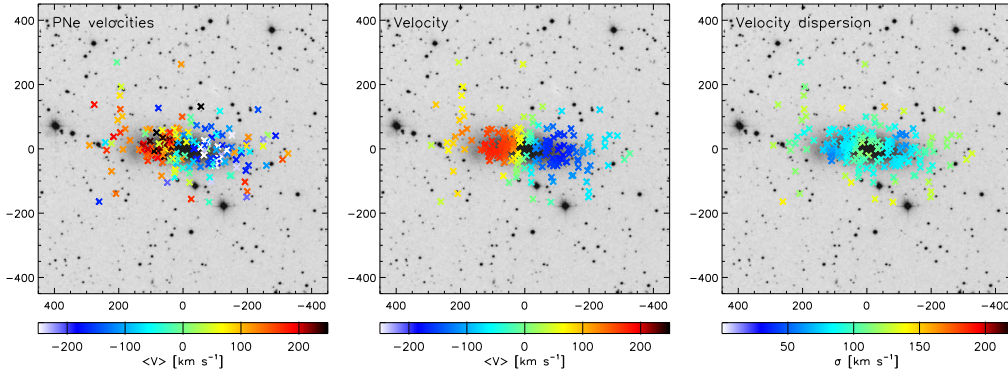


Figure 1. Recovering the kinematics of the PNe population from individual radial velocities. The left panel shows the position of the PNe (crosses) detected in NGC 1023, superimposed to the image of the field of view (data from Noordermeer et al. 2008). The color of each cross is proportional to the radial velocity of the PNe (minus the galaxy systemic velocity), as indicated by the color bar. The central and right panels show the values of the reconstructed velocity and velocity dispersion fields at each PNe position, using the adaptive Gaussian kernel smoothing. The spatial scale is in arcseconds.

regions where these tracers overlap. Moreover, for early-type galaxies, the PNe spatial distribution is consistent with the extrapolation of the Sérsic fit to the stellar surface brightness, rather than a de Vaucouleurs plus an exponential disk, in line with the view of “spheroidal” halos around early-type galaxies, rather than “disk-like” structures (e.g. Coccato et al. 2009, and references therein).

These findings have an important practical application: the combined information of the kinematics and distribution of stars (that typically probe the central effective radius) and PNe (in the outer regions) can be used to derive the entire dynamic picture of a galaxy and its halo (see Section 3.2.1).

There are, however, few exceptions to this picture. The most outstanding example is given by E6 galaxy NGC 821 (Figure 2). Its PNe system (Coccato et al. 2009) shows a rotation axis which is $\sim 100^\circ$ misaligned from that of the stars (Proctor et al. 2009; Foster et al. 2016). These exceptions and, more in general, the differences between the kinematics obtained from different tracers, are seen as an indication of recent satellite accretion in the halos (Coccato et al. 2013; Foster et al. 2014; Romanowsky et al. 2014; Longobardi et al. 2015).

3. Results

3.1. Early works

3.1.1. The Milky-Way

The use of PNe radial velocities to measure the kinematic properties of a galaxy was first applied to our own Milky Way. In their pioneering work, Schneider & Terzian (1983) exploited the measured radial velocities of 252 galactic PNe to derive the galactic rotation curve beyond the solar circle. Their results showed a rising rotation curve out to ~ 15 kpc, in agreement and extending further out, the previous results obtained with O-B stars and CO clouds.

The study was extended also to the MW bulge by Durand et al. (1998) using 867 galactic PNe and later by Beaulieu et al. (2000) using 373 bulge PNe. At odds with previous results, there was no evidence for a rising disk rotation curve in these studies.

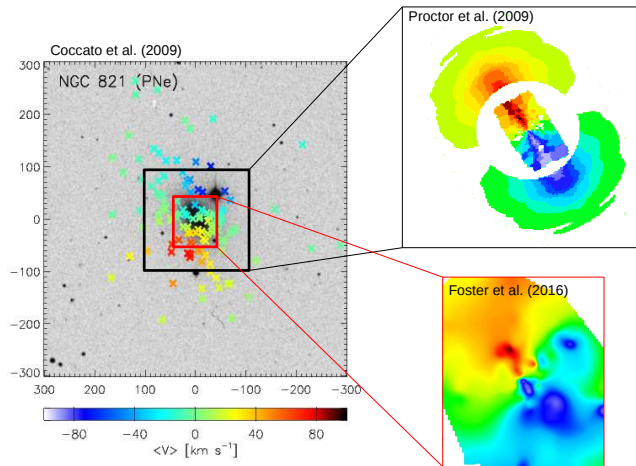


Figure 2. Comparison between the velocity field of the PNe population (left panel) compared with the velocity field of the stars (right panels). PNe data are from Coccato et al. (2009), stellar data are from Proctor et al. (2009, for the inner $\sim 200'' \times 200''$) and Foster et al. (2016, for the inner $\sim 100'' \times 120''$). The direction of rotation of PNe is $\sim 100^\circ$ misaligned with respect to the direction of rotation of the stars. The spatial scale on the left panel is in arcseconds.

The kinematic of the bulge was found to be consistent with a linearly increasing rotation velocity (Durand et al. 1998). The comparison with N-body models showed that the kinematics of the bulge is consistent with models where the MW bulge and bar formed from the disk via bar-forming instabilities (Beaulieu et al. 2000).

Nowadays, the census of galactic PNe with radial velocities includes about 2500 objects (e.g., the HASH database, Parker et al. 2016).

3.1.2. The Andromeda Galaxy M31

The next obvious candidate for these studies was our neighbor galaxy M31. Nolthenius & Ford (1987) detected and measured the radial velocities of 37 PNe within 15 and 30 kpc along the photometric major axis of M31. Despite the scatter in their measurements, they showed that the rotation curve of M31 flattens at $\sim 220 \text{ km s}^{-1}$ outside 20 kpc from the galaxy center. The first quantum step in the number of PNe detection in M31 and its satellites was done in Merrett et al. (2006), with the publication of a catalog of ~ 2700 sources. This catalog allowed to identify a new satellite (Andromeda VIII) and to probe the stellar distribution in M31 out to large distance from the galaxy center: they found no indication of a cut-off in M31's disk out to four scale lengths, and no signs of a spheroidal halo population in excess of the bulge out to 10 effective bulge radii.

3.2. Early-Types

The use of PNe radial velocity measurements has revealed the following kinematic properties for the halos of early-type galaxies (e.g., Douglas et al. 2007; Coccato et al. 2009; Teodorescu et al. 2010; McNeil et al. 2010, and references therein):

- The velocity dispersion and V_{RMS} have a large variety of radial profiles, including flat profiles (generally associated to more massive galaxies), declining profiles (generally associated to less massive ellipticals), and even rising profiles (generally associated to lenticulars with a prominent stellar halo, or disturbed systems).
- Kinematic twists and misalignment in the velocity fields are more frequent at large

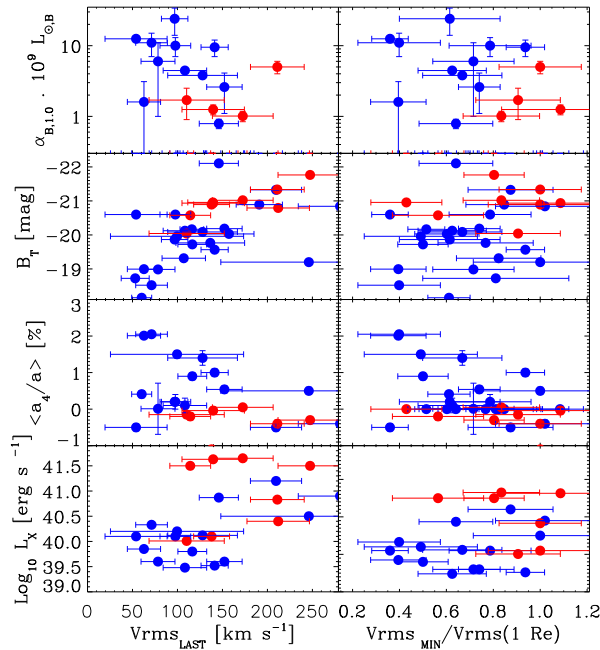


Figure 3. Correlations between the halo kinematics and other galaxy properties (updated from Coccato et al. 2009). The halo kinematics is parametrized with the outermost value of V_{TMS} (left) and its normalization at 1 effective radius (right), as obtained from PNe radial velocities. Each point represents a galaxy. From top to bottom, the panels indicate: PNe specific frequency, total B-band luminosity, shape parameter, and total X-ray luminosity. Galaxies that are classified as fast rotators are shown in blue, slow rotators in red.

radii than what observed in the inner regions. Twists are also observed in some fast rotator galaxies.

- Outer halos are characterized by more complex radial profiles of the specific angular momentum-related $\lambda(R)$ parameter than observed within one effective radius. Some galaxies are more rotational dominated at large radii than in their central parts (i.e., the $\lambda(R)$ profile increase in the halo), some other are pressure supported at large radii (i.e., the $\lambda(R)$ profile decreases in the halo).

- The halo kinematics are correlated with other galaxy properties, such as total B-band and X-ray luminosity, isophotal shape, total stellar mass, V/σ and PNe specific frequency, with a clear separation between fast and slow rotators (Figure 3).

- That the halos of massive ellipticals sometimes host kinematic substructures, interpreted as relics of accretion events. Kinematic substructures are also found in the halos of spiral galaxies (e.g., Herrmann et al. 2009).

3.2.1. Mass distribution in Early-Type galaxies: “lost and found” Dark Matter

The main science driver for studying the kinematics of PNe in Early-Type galaxies is to use them as tracer for the gravitational potential in order to infer the mass distribution and the fraction of dark matter.

Initial works that included a significant amount of PNe in the analysis were carried on massive nearby ellipticals, such as NGC 1316 (Arnaboldi et al. 1998), NGC 5128 (Hui et al. 1995; Peng et al. 2004), and more recently on NGC 4649 (Teodorescu et al. 2011) - just to cite few examples. The signature of the presence of dark matter was

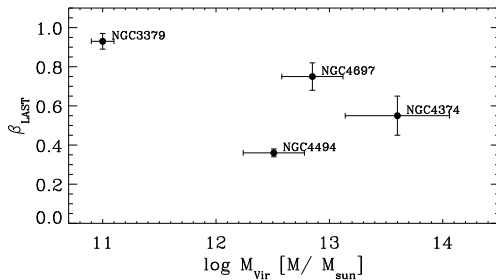


Figure 4. Trend between virial mass (from Forbes et al. 2017, Table 1) and anisotropy parameter β (from Fig. 23 in Morganti et al. 2013, and from Fig. A2 in Napolitano et al. 2011). The value of β refers to the outermost determination. Radially biased orbits are those with high values of β ; isotropic models have $\beta = 0$.

clearly present in the kinematic profile at large radii. Other works led by several team that combined the information of other tracers to the PNe, reached similar results (e.g., Napolitano et al. 2005; Deason et al. 2012; Forbes et al. 2016).

Controversial results emerged from the study of ordinary ellipticals. Studies by Ciardullo et al. (1993); Méndez et al. (2001, 2009); Romanowsky et al. (2003) indicated that the kinematic profile of intermediate luminosity ellipticals are consistent with no dark matter, or much less that what predicted by the Λ CDM model. The different teams adopted different modeling techniques, including isotropic or constant anisotropic Jeans models fitting several moments of the PNe velocity distribution, which lead to results consistent to each others. These findings challenged not only the view that *all* galaxies are embedded in massive halos, but also alternative theories such as MOND (Milgrom 1983), that were not able to reconcile the luminous mass in these galaxies with the observed decreasing velocity dispersion profiles.

The solution was found by assuming that the stellar orbits are anisotropic, and that their anisotropy varies with radius (becoming more radial outward). This reconciled the observed dispersion profiles with MOND (Milgrom & Sanders 2003). Moreover the increase of radial anisotropy at large radii is consistent with the numerical simulations of disk-galaxy mergers in a Λ CDM universe (Dekel et al. 2005).

Following this idea, more elaborated dynamical models of PNe datasets revealed that the inclusion of radial variation in the anisotropy profile was indeed able to reconcile the dark matter content in low-luminous ellipticals with the predictions of Λ CDM, although a certain amount of degeneracy between mass, shape, and anisotropy exists for nearly spherical systems (e.g., de Lorenzi et al. 2009). In addition, as indicated in Figure 4, the new models suggest that lower mass halos have stars in orbits that have higher radial anisotropy than the stars in high mass halos (Morganti et al. 2013, Napolitano et al. 2011, Napolitano, priv. comm.), in line with what found also using other tracers (e.g., Zhu et al. 2016).

3.3. Lenticulars

Lenticular galaxies are mainly composed by a spheroid and a disk without spiral arms. Therefore, it is reasonable to assume that some PNe are associated to the spheroid and some to the disk. The association of a PNe to one component or the other can be done by combining the surface brightness spheroid/disk decomposition with PNe kinematic data, assuming a non rotating model for the spheroid component (Cortesi et al. 2011). One application is to recover the disk kinematics by removing the contamination from

the PNe associated to the spheroid in order to study scaling relations such as the Tully-Fisher at large radii. Cortesi et al. (2013) found that: i) the disks of S0s have higher velocity dispersion than the spirals with the same rotational velocity; and that ii) S0s lie around one magnitude below the Tully-Fisher relation for spiral galaxies, i.e., disks of S0s have higher circular velocity than those of spirals of the same luminosity. This was interpreted by the authors as an indication of a mild harassment process that heated disks of spirals and transformed them into S0s.

3.4. Spirals

Although spiral galaxies have gas that can be used to probe their kinematics and mass distribution at large radii, PNe are still useful to probe the vertical stellar velocity dispersion (σ_Z) in nearly face-on systems. Herrmann & Ciardullo (2009) studied a sample of five nearby, low-inclination spiral galaxies. They found that: i) 4/5 spirals have constant mass-to-light ratio out to ~ 3 optical scale lengths (h_Z); ii) outside $\sim 3h_Z$, σ_Z becomes flat with radius; iii) the disks of early type spirals have higher values of mass-to-light ratio and are closer to maximal than the disks of later-type spirals; iv) the inner halos of spirals are better fit by pseudo-isothermal laws than by NFW models.

The PNe in spiral galaxies were also used to measure the stellar migration in stellar disks to investigate its influence on the variation of metallicity gradients in stellar disks with time (Magrini et al. 2016).

4. Summary

In this review I have illustrated the main findings obtained by using planetary nebulae as kinematic tracers in galaxy halos, sometimes pursuing an historical approach. The main lessons that we can learn in these last decades on the topics are:

- In the regions where PNe and absorption line data overlap, PNe well trace the surface brightness and kinematics of stars (with few exceptions). Therefore, PNe can be used to measure the properties of galaxy halos by extending the information of stellar kinematics to large radii, and to unveil signatures of accretions events also in galaxies with a relatively undisturbed morphology.
- Variable radial anisotropy needs to be considered in dynamical models in order to obtain a reliable estimate of the dark matter content and distribution in the halos. There is the indication lower mass halos have stars in orbits that have higher radial anisotropy than the stars in high mass halos.
- The properties of the PNe population in spiral galaxies suggest that the disks of early type spirals have higher values of mass-to-light ratio and are closer to maximal than the disks of later-type spirals.
- The study of PNe kinematics in S0 galaxies revealed that disks of S0s have higher velocity dispersion than those of spirals, and that S0s lie one magnitude below the Tully-Fisher relation with respect to spiral galaxies of the same luminosity.

References

- Amorisco, N. C. & Evans, N. W. 2012, MNRAS, 424, 1899
 Arnaboldi, M. 2012, in IAU Symposium, Vol. 283, IAU Symposium, 267–274
 Arnaboldi, M., Freeman, K. C., Gerhard, O., et al. 1998, ApJ, 507, 759
 Arnold, J. A., Romanowsky, A. J., Brodie, J. P., et al. 2014, ApJ, 791, 80
 Beaulieu, S. F., Freeman, K. C., Kalnajs, A. J., Saha, P., & Zhao, H. 2000, AJ, 120, 855
 Binney, J. & Tremaine, S. 1987, Galactic dynamics

- Ciardullo, R., Jacoby, G. H., & Dejonghe, H. B. 1993, *ApJ*, 414, 454
- Coccatto, L., Arnaboldi, M., & Gerhard, O. 2013, *MNRAS*, 436, 1322
- Coccatto, L., Arnaboldi, M., Gerhard, O., et al. 2010a, *A&A*, 519, A95
- Coccatto, L., Gerhard, O., & Arnaboldi, M. 2010b, *MNRAS*, 407, L26
- Coccatto, L., Gerhard, O., Arnaboldi, M., et al. 2009, *MNRAS*, 394, 1249
- Coccatto, L., Gerhard, O., Arnaboldi, M., & Ventimiglia, G. 2011, *A&A*, 533, A138
- Cortesi, A., Merrifield, M. R., Arnaboldi, M., et al. 2011, *MNRAS*, 414, 642
- Cortesi, A., Merrifield, M. R., Coccatto, L., et al. 2013, *MNRAS*, 432, 1010
- de Lorenzi, F., Gerhard, O., Coccatto, L., et al. 2009, *MNRAS*, 395, 76
- Deason, A. J., Belokurov, V., Evans, N. W., & McCarthy, I. G. 2012, *ApJ*, 748, 2
- Dekel, A., Stoehr, F., Mamon, G. A., et al. 2005, *Nature*, 437, 707
- Douglas, N. G., Arnaboldi, M., Freeman, K. C., et al. 2002, *PASP*, 114, 1234
- Douglas, N. G., Napolitano, N. R., Romanowsky, A. J., et al. 2007, *ApJ*, 664, 257
- Durand, S., Acker, A., & Zijlstra, A. 1998, *A&AS*, 132, 13
- Forbes, D. A., Alabi, A., Romanowsky, A. J., et al. 2016, *MNRAS*, 458, L44
- Forbes, D. A., Alabi, A., Romanowsky, A. J., et al. 2017, *MNRAS*, 464, L26
- Foster, C., Arnold, J. A., Forbes, D. A., et al. 2013, *MNRAS*, 435, 3587
- Foster, C., Lux, H., Romanowsky, A. J., et al. 2014, *MNRAS*, 442, 3544
- Foster, C., Pastorello, N., Roediger, J., et al. 2016, *MNRAS*, 457, 147
- Greene, J. E., Janish, R., Ma, C.-P., et al. 2015, *ApJ*, 807, 11
- Greene, J. E., Murphy, J. D., Comerford, J. M., Gebhardt, K., & Adams, J. J. 2012, *ApJ*, 750, 32
- Herrmann, K. A. & Ciardullo, R. 2009, *ApJ*, 705, 1686
- Herrmann, K. A., Ciardullo, R., & Sigurdsson, S. 2009, *ApJ*, 693, L19
- Hui, X., Ford, H. C., Freeman, K. C., & Dopita, M. A. 1995, *ApJ*, 449, 592
- Jacoby, G. H. 1980, *ApJS*, 42, 1
- Longobardi, A., Arnaboldi, M., Gerhard, O., & Mihos, J. C. 2015, *A&A*, 579, L3
- Magrini, L., Coccatto, L., Stanghellini, L., Casasola, V., & Galli, D. 2016, *A&A*, 588, A91
- McNeil, E. K., Arnaboldi, M., Freeman, K. C., et al. 2010, *A&A*, 518, A44
- Méndez, R. H., Riffeser, A., Kudritzki, R.-P., et al. 2001, *ApJ*, 563, 135
- Méndez, R. H., Teodorescu, A. M., Kudritzki, R.-P., & Burkert, A. 2009, *ApJ*, 691, 228
- Merrett, H. R., Merrifield, M. R., Douglas, N. G., et al. 2006, *MNRAS*, 369, 120
- Milgrom, M. 1983, *ApJ*, 270, 365
- Milgrom, M. & Sanders, R. H. 2003, *ApJ*, 599, L25
- Morganti, L., Gerhard, O., Coccatto, L., Martinez-Valpuesta, I., & Arnaboldi, M. 2013, *MNRAS*, 431, 3570
- Napolitano, N. R., Capaccioli, M., Romanowsky, A. J., et al. 2005, *MNRAS*, 357, 691
- Napolitano, N. R., Romanowsky, A. J., Capaccioli, M., et al. 2011, *MNRAS*, 411, 2035
- Nolthenius, R. & Ford, H. C. 1987, *ApJ*, 317, 62
- Noordermeer, E., Merrifield, M. R., Coccatto, L., et al. 2008, *MNRAS*, 384, 943
- Parker, Q. A., Bojčić, I. S., & Frew, D. J. 2016, *Journal of Physics Conference Series*, 728, 032008
- Peng, E. W., Ford, H. C., & Freeman, K. C. 2004, *ApJ*, 602, 685
- Proctor, R. N., Forbes, D. A., Romanowsky, A. J., et al. 2009, *MNRAS*, 398, 91
- Romanowsky, A. J., Arnold, J. A., Brodie, J. P., et al. 2014, in *Astronomical Society of the Pacific Conference Series*, Vol. 486, *Multi-Spin Galaxies*, ASP Conference Series, ed. E. Iodice & E. M. Corsini, 169
- Romanowsky, A. J., Douglas, N. G., Arnaboldi, M., et al. 2003, *Science*, 301, 1696
- Romanowsky, A. J. & Kochanek, C. S. 2001, *ApJ*, 553, 722
- Schneider, S. E. & Terzian, Y. 1983, *ApJ*, 274, L61
- Teodorescu, A. M., Méndez, R. H., Bernardi, F., Riffeser, A., & Kudritzki, R. P. 2010, *ApJ*, 721, 369
- Teodorescu, A. M., Méndez, R. H., Bernardi, F., et al. 2011, *ApJ*, 736, 65
- Zhu, L., Romanowsky, A. J., van de Ven, G., et al. 2016, *MNRAS*, 462, 4001